molecules

MDPI

Communication

Detection and Verification of a Key Intermediate in an Enantioselective Peptide Catalyzed Acylation Reaction

Matthias Brauser, Tim Heymann and Christina Marie Thiele *

Clemens-Schöpf-Institute for Organic Chemistry and Biochemistry, Department of Chemistry, Technical University of Darmstadt, Alarich-Weiss-Straße 4, 64287 Darmstadt, Germany

* Correspondence: cthiele@thielelab.de

Abstract: Until now, the intermediate responsible for the acyl transfer of a highly enantioselective tetrapeptide organocatalyst for the kinetic resolution of trans-cycloalkane-1,2-diols has never been directly observed. It was proposed computationally that a π-methylhistidine moiety is acylated as an intermediate step in the catalytic cycle. In this study we set out to investigate whether we can detect and characterize this key intermediate using NMR-spectroscopy and mass spectrometry. Different mass spectrometric experiments using a nano-ElectroSpray Ionization (ESI) source and tandem MS-techniques allowed the identification of tetrapeptide acylium ions using different acylation reagents. The complexes of *trans*-cyclohexane-1,2-diols with the tetrapeptide were also detected. Additionally, we were able to detect acylated tetrapeptides in solution using NMR-spectroscopy and monitor the acetylation reaction of a *trans*-cyclohexane-1,2-diol. These findings are important steps towards the understanding of this highly enantioselective organocatalyst.

Keywords: acylation; imidazolium ion; mass spectrometry; NMR spectroscopy; organocatalysis

Citation: Brauser, M.; Heymann, T.; Thiele, C.M. Detection and Verification of a Key Intermediate in an Enantioselective Peptide Catalyzed Acylation Reaction. *Molecules* **2022**, *27*, 6351. https://doi.org/10.3390/molecules27196351

Academic Editors: Nives Galić and Ana Čikoš

Received: 18 August 2022
Accepted: 20 September 2022
Published: 26 September 2022

1. Introduction

The selective acyl transfer onto alcohols is important for various signaling pathways in nature. Plants use acetyl transferases to synthesize volatile esters during fruit ripening. Mammals on the other hand use it to produce neurotransmitters such as acetylcholine [1,2].

The enzyme-substrate interactions involving intermolecular hydrogen bonds or hydrophobic effects inside the pockets of enzymes inspired chemists to develop catalysts that mimic these functions [3–5]. By reducing the rather complex enzyme pockets to smaller peptides Miller et al. introduced oligo-peptides that were able to transfer acyl groups from acetic anhydride onto racemic alcohols, producing enantiomeric excess in the acylated product. This reactivity was attributed to the π-methylhistidine moiety and hydrogen bonds stabilizing the catalysts structure [6–10]. An important step forward was published in 2008 by the Schreiner group. The less flexible tetrapeptide (TP) Boc-L(π-Me)-His^{A}Gly-L-Cha-L-Phe-OMe **1** enabled enantiomeric excess values of >99% for the acetylation of racemic *trans*-cycloalkane-1,2-diols (rac)-**2** in toluene (See Scheme 1) [11]. In addition to toluene other solvents were tested for this highly enantioselective kinetic resolution of (rac)-**2**. The use of dichloromethane (DCM) and trifluoromethylbenzene resulted in lower conversion and significantly lowered the selectivity, while almost no conversion or selectivity was observed in acetonitrile [11]. Later investigations explored the scope of other electrophiles as well. Using, e.g., isobutyric anhydride **4** as an electrophile the reaction still showed high selectivity and enantiomeric excess values, while for trimethylacetic anhydride **5** almost no conversion and selectivity were observed. This was attributed to steric hindrance [12].

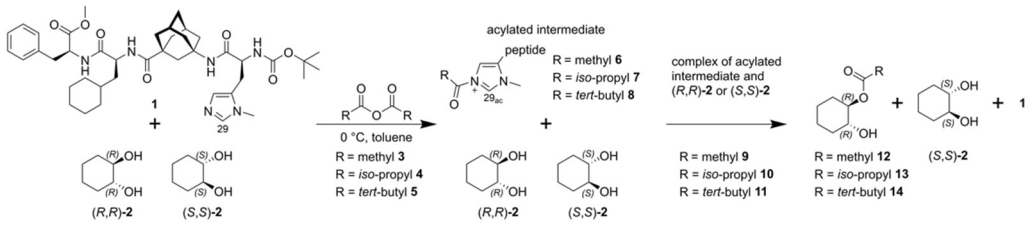

Scheme 1. Generalized reaction scheme of tetrapeptide **1** with *trans*-cyclohexane-1,2-diols (*R*,*R*)-**2** and (*S*,*S*)-**2** in toluene including the proposed catalytically active acylium ion intermediates (**6**, **7**, and **8**) using different acylation reagents [11,12]. For the sake of completeness, the proposed transient complexes of **6**–**8** with the diols are indicated as **9**–**11** and the acetylated products of (*R*,*R*)-**2** are shown as **12**–**14**.

The high enantioselectivity was proposed to originate from a pocket-like structure formed by tetrapeptide **1** as a result of incorporating γ-aminoadamantane carboxylic acid into the peptide. This building block increased the stiffness of the peptide backbone while promoting enantiospecific interactions of the *trans*-cycloalkane-1,2-diols (rac)-**2** and the catalytically active π-methylhistidine moiety [11]. Calculated transition states for the acylation of racemic *trans*-cyclohexane-1,2-diols using Density-Functional Theory (DFT) conducted by Shinisha et al. favor the *R*,*R* configured transition state, in accordance with the experiment [13]. The obtained transition state structures resemble the previously proposed pocket-like arrangement of the peptide and the *trans*cyclohexane-1,2-diols. To account for dispersion interactions between catalyst and substrate in the calculations, Müller et al. published a DFT reoptimized pocket-like structure of the acetylated peptide using a functional parametrized for medium range correlations [14]. The ring of the *trans*-cyclohexane-1,2-diol in this model is in close proximity to the cyclohexane moiety of the peptide [12,15]. This predicted interaction could later be correlated with an experimentally observed Nuclear Overhauser Effect (NOE) [16] contact between the cyclohexane moiety of tetrapeptide **1** and (1*R*,2*R*)-cyclohexane-1,2-diol (*R*,*R*)-**2**. In the same work a solution conformer ensemble of the unacylated tetrapeptide **1** was established using NOE and Residual Dipolar Coupling (RDC) data affirming pocket-like conformations to be present in solution for **1** [17].

In the mechanism proposed for the reaction of tetrapeptide **1** and the *trans*-cyclohexane-1,2-diols (rac)**-2**, the π-methylhistidine moiety is supposed to transfer the acyl group onto the diols. Thus far, acylated intermediates of tetrapeptide **1** (structures 6–8 in Scheme 1) have not yet been observed experimentally. Alachraf et al. were able to detect a related, acylated tetrapeptide using High Resolution ElectroSpray Ionization Mass Spectrometry (ESI-HRMS) [18].

We therefore set out to investigate if we can spectroscopically detect different tetrapeptide acylium ions—using three of the previously employed anhydrides (**3**, **4** and **5**)—in toluene and DCM using ESI-HRMS [19,20] and confirm the covalent nature of these intermediates as well as their reactivity using Nuclear Magnetic Resonance (NMR)-spectroscopy. Additionally, the complexation of *trans*-cyclohexane-1,2-diols (rac)-**2** with tetrapeptide **1** and the acetylated intermediate **6** was investigated using nano-ESI-HRMS.

2. Results and Discussion

2.1. ESI-HRMS Measurements

As a starting point we used a solution of tetrapeptide **1** in DCM and added anhydride **3** in excess to form the corresponding acetylated tetrapeptide **6**. By spraying this solution into a mass spectrometer recording in positive ion mode, a full scan ESI-HRMS spectrum was obtained. The acetylated tetrapeptide **6** was validated using a Higher-Energy Collision Dissociation (HCD) fragment spectrum of precursor ion **6** as shown in Figure 1. (for more details see supporting information; Section S2.0, Figure S1).

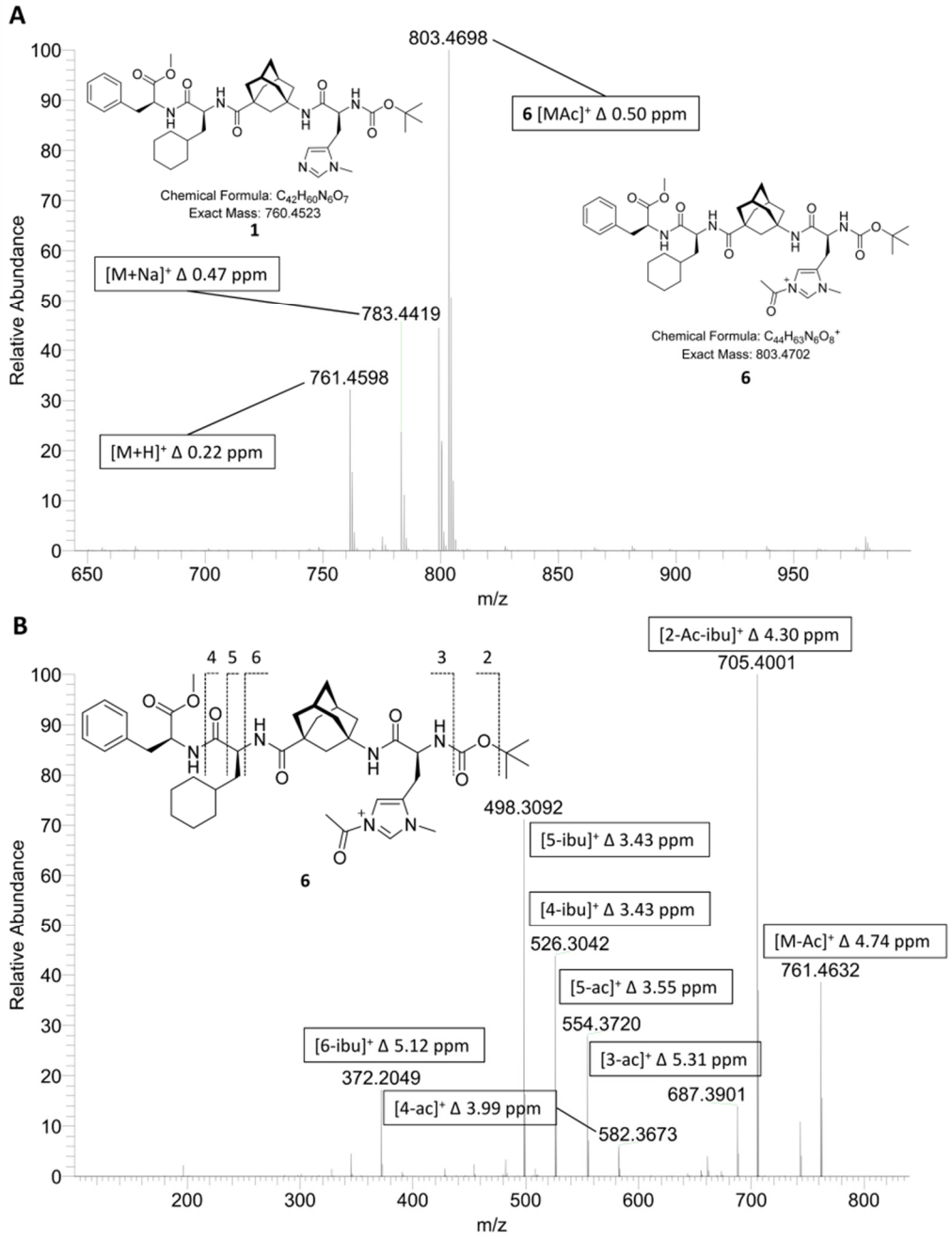

Figure 1. (**A**) Excerpt of full scan positive ion mode (ESI^+) spectrum of a 1 mg/mL solution of tetrapeptide **1** in DCM with 1% anhydride **3** and 1% acetic acid **15**. (**B**) HCD fragment spectrum of the acetylated tetrapeptide **6** with annotated characteristic fragments and their respective mass error.

After formation of acetylated tetrapeptide **6** was detected and validated, we repeated the experiment with anhydrides **3**, **4**, and **5** in DCM and toluene, successfully detecting the expected masses of the corresponding acylium ions under all conditions with a mass error of smaller 5 ppm (See Table 1).

Table 1. Calculated and observed masses for the cations.

Formula	6 $(C_{44}H_{63}N_6O_8)^+$	7 $(C_{46}H_{67}N_6O_8)^+$	8 $(C_{47}H_{69}N_6O_8)^+$
exact mass	803.4702	831.5015	845.5171
Δ (DCM)/ppm	0.50	0.60	−4.97
Δ (toluene)/ppm	0.87	−0.60	1.54

The intensities of the cations found follow the experimentally observed trend of reactivity in the acylation of the trans-cyclohexane-1,2-diols: The acetylated tetrapeptide **6** displayed the highest ion count, followed by the isobutyrylated tetrapeptide **7**, and, with very little observed ions, the pivalylated tetrapeptide **8** [12]. Fragmentation of ions selected in MS^2 experiments was carried out to confirm the identity of the respective ions (See supporting information Figures S2 and S3 for spectra).

After the successful detection of the acylated tetrapeptides **6**, **7**, and **8** the acyl transfer onto *trans*-cyclohexane-1,2-diols was investigated by ESI-HRMS in the negative ion mode. Here, it would be intriguing if the non-covalent interactions between tetrapeptide **1** (or acetylated tetrapeptide **6**) and the diol **2** or the respective acetylated diol **12** could be detected by MS. For this, solutions of tetrapeptide **1** and either *R*,*R*-*trans*-cyclohexane-1,2-diol (*R*,*R*)**-2** or *S*,*S*-*trans*-cyclohexane-1,2-diol (*S*,*S*)**-2** in DCM with 1% acetic anhydride **3** and 1% acetic acid **15** were prepared. DCM was used as a solvent in this case to increase the concentration, since the solubility of tetrapeptide **1** in DCM is higher than in toluene. The addition of acetic acid **15** to the solutions improved the ionization of the molecules (Figure 2).

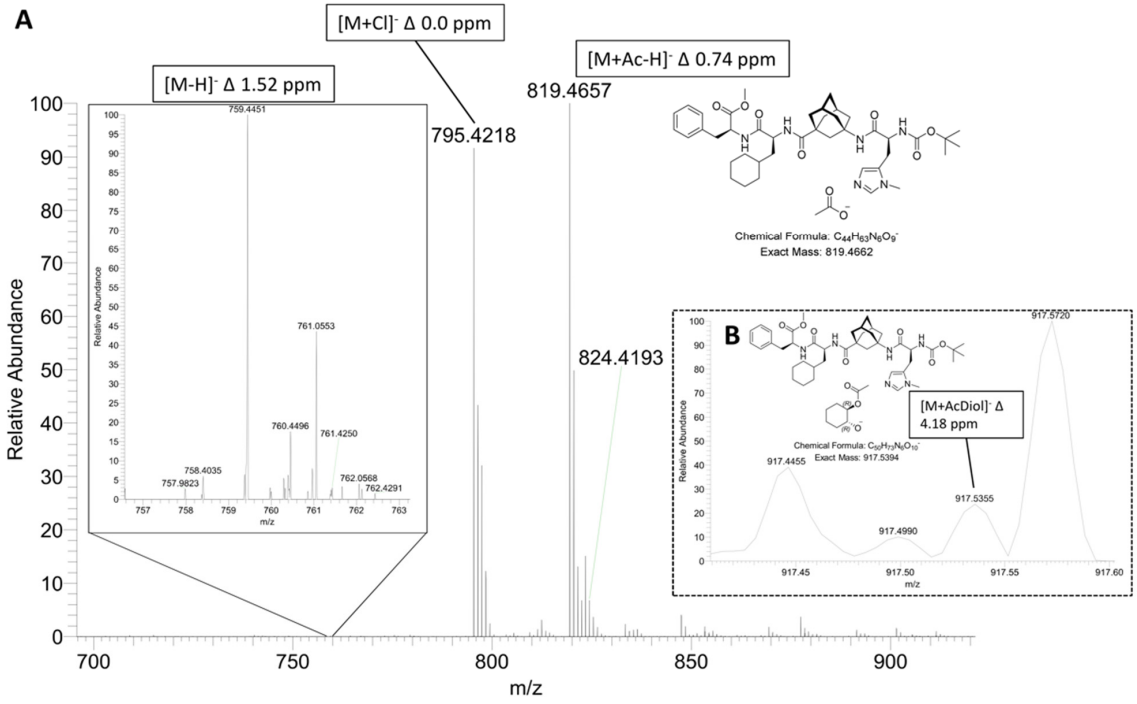

Figure 2. (**A**) Excerpt of full negative ion mode (ESI^-) spectrum of tetrapeptide **1** with 1% acetic anhydride **4** and 1% acetic acid **15** sprayed from DCM. Insert of zoom on $[M-H]^-$ ion of tetrapeptide **1** (m/z = 759.4451). (**B**) Selected Ion Monitoring (SIM) of m/z = 917.5 of tetrapeptide **1** with acetic anhydride **3** as well as *R*,*R*-*trans*-cyclohexane-1,2-diol (*R*,*R*)**-2** sprayed from DCM. Important ions are annotated with their respective masses and mass errors. One possible charge localization of $[M+AcDiol]^-$ is shown; others are possible.

In this experiment the $[M-H]^-$ ion of tetrapeptide **1** (m/z = 759.4451) is only present in small amounts, the acetate adduct $[M+Ac-H]^-$ can be easily detected with high signal to noise ratio at m/z = 819.4657. Additionally, an ion, the mass of which is in-line with a complex between tetrapeptide **1** and the acetylated diol **12** (called reaction product complex from now on) can be observed by SIM of its precursor mass m/z = 917.53 in very low abundance. The composition of this ion is validated by matching the fragments of the HCD spectra of tetrapeptide **1** with those of the detected precursor mass of the reaction product complex as shown in Figure 3 (See supporting information Figure S4 for equivalent experiment using *S*,*S*-*trans*-cyclohexane-1,2-diol (*S*,*S*)**-2**).

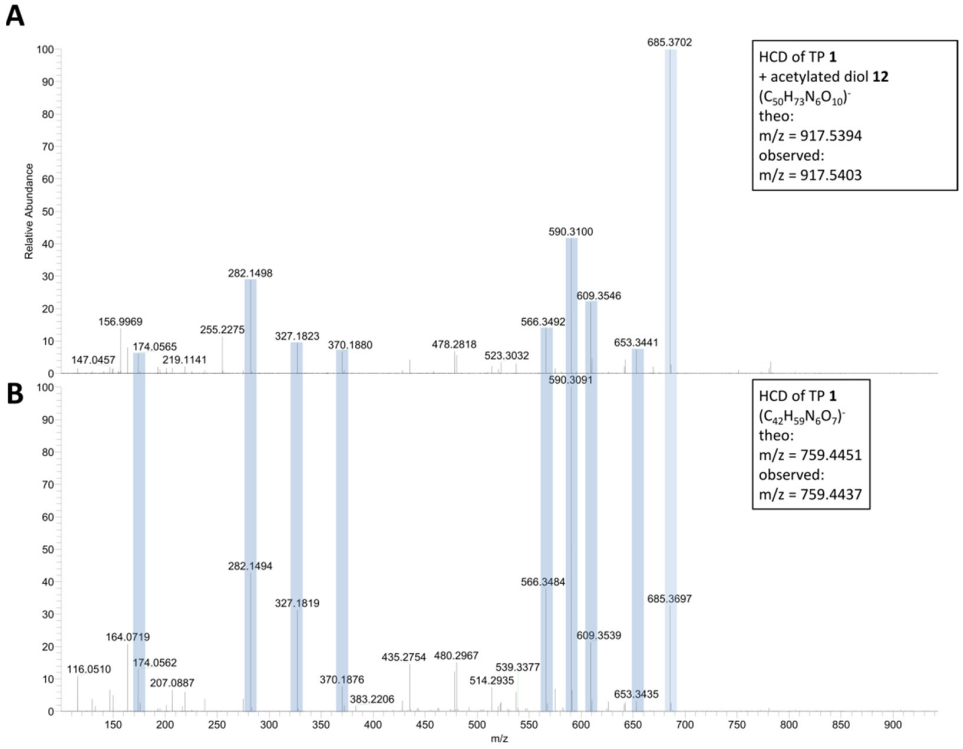

Figure 3. HCD of the reaction product complex with m/z = 917.53 (**A**) and HCD of **1** m/z = 759.44 (**B**) with equivalent fragment masses accentuated by light blue color. Stacked plot of negative ion mode (ESI^-) spectra of tetrapeptide **1** with acetic anhydride **3** as well as *R*,*R*-*trans*-cyclohexane-1,2-diol (*R*,*R*)**-2** (**A**) and **1** alone (**B**), sprayed from DCM.

The obtained HRMS fragment masses can be assigned to tetrapeptide **1** as their parent structure (the fragments observed were the same as in toluene for the acetate adduct of **1** with m/z = 819.4667 (See supporting information Figure S5)). This shows that the detected ions of the complex with m/z = 917.5394 contained tetrapeptide **1**. To further analyze the reaction product complex HCD dissociation curves of the complex at m/z = 917.53 as well as the adduct complex of tetrapeptide **1** and acetic acid **15** were acquired to allow a relative comparison of their stability (Figure 4).

After a DoseResp [21] fit using Origin (Pro), version number 9.8.0 [22], employing equation Equation (1), the E_{50} value is obtained, where A1 equals the bottom asymptote, A2 the top asymptote, E_{50} the center and p the Hill slope of the curve.

$$y = A1 + \frac{A2 - A1}{1 + 10^{(E_{50} - x)p}} \quad (1)$$

The E_{50} value corresponds to the normalized collision energy (NCE) needed to dissociate 50% of the complex and can be used as a measure of the relative stability of the complex [23]. For TP **1** + acetate an E_{50} of 12.5 NCE is obtained while for the reaction product complex an E_{50} of 13.5 NCE is determined. The difference of 1 NCE between the two E_{50} correlates with higher binding affinities between tetrapeptide **1** and acetylated diol **12** in contrast to the acetate adduct of tetrapeptide **1** [24]. Since electrostatics play a large role in the interactions between molecules in ESI-MS measurements [20], the high electron density on the oxygen-atoms of **12** or **2** allows for strong interactions with **1**, e.g., through hydrogen bonding that is preserved over the measurement. We could thus theorize that the delocalized charge of the acetate ion interacts less strongly with **1**. Hence, the higher binding affinity with the already acetylated product **12**, supports the hypothesis that during the acetylation of the diol (*R*,*R*)**-2** a complex is formed either with tetrapeptide **1** or the acetylated tetrapeptide **6** before the acyl residue is transferred onto diol (*R*,*R*)-**2**. Thus, the

detection of the acylium ions **6**, **7** and **8**, as well as the complexes of the acetylated diols and tetrapeptide **1** using HRMS was successful.

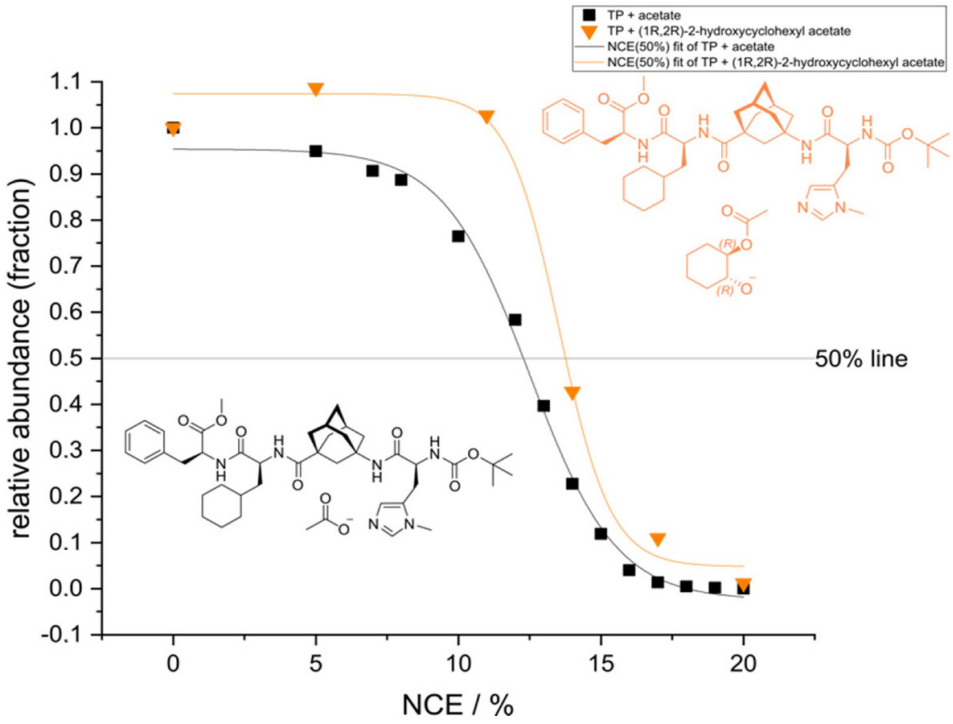

Figure 4. DoseResp [21] fit of relative abundance in dependence of normalized collision energy (NCE) of TP **1** + acetate, m/z = 819.47 (black) and reaction product complex (TP **1** + acetylated diol **12**), m/z = 917.53 (orange). One possible charge localization of $[M+AcDiol]^-$ is shown; others are possible.

2.2. NMR Measurements

To provide further evidence for the existence and connectivity of the acylated tetrapeptides in solution various NMR experiments were performed on solutions of tetrapeptide **1** and the anhydrides **6**, **7**, and **8** in DCM-d_2 (See supporting information Table S1 for more details on sample compositions). First of all, resonances indicative of the formation of the acylated tetrapeptides need to be observed. Considering that there are no previously published NMR spectra of the acylated tetrapeptides and the low ion count observed in the MS measurements, the effective concentration of the acylium ion in solution appears to be low. DCM was again used as a solvent to increase the concentration. Figure 5 shows the changes in the ^{1}H-NMR spectrum upon addition of acetic anhydride **3** to tetrapeptide **1** in DCM-d_2.

In addition to several chemical shift changes of tetrapeptide resonances, especially for the amide protons, signals of acetic acid **15** and acetic anhydride **3** become apparent. Further, the highlighted new signal at 10.5–10.6 ppm is notable. A similar signal was found in a solution of isobutyric anhydride **4** and tetrapeptide **1** but no signal in this shift range was observed for trimethylacetic anhydride **5**, congruent with the low reactivity of **5** observed in reactions by the Schreiner group (See supporting information Figures S6 and S7 for spectra) [12]. As the chemical shift is in accordance with protons in similar chemical environments in imidazolium-based ionic liquids in organic solvents, the signal observed is proposed to belong to $H29_{ac}$ [25]. To obtain further evidence of the connectivity in the acylation site the ^{13}C-chemical shift of the respective carbon $C29_{ac}$ needs to be obtained. The ^{1}H-^{13}C-Heteronuclear Single Quantum Coherence (HSQC) [26] spectrum shows a correlation to a carbon chemical shift of 139 ppm for $H29_{ac}$, while carbon C29 of the unacetylated tetrapeptide **1** has a ^{13}C-chemical shift of 137 ppm in the same spectrum (See supporting information Figure S8 for ^{1}H-^{13}C-HSQC). Thus, carbon $C29_{ac}$ is attributed to the signal with a chemical shift of 139 ppm.

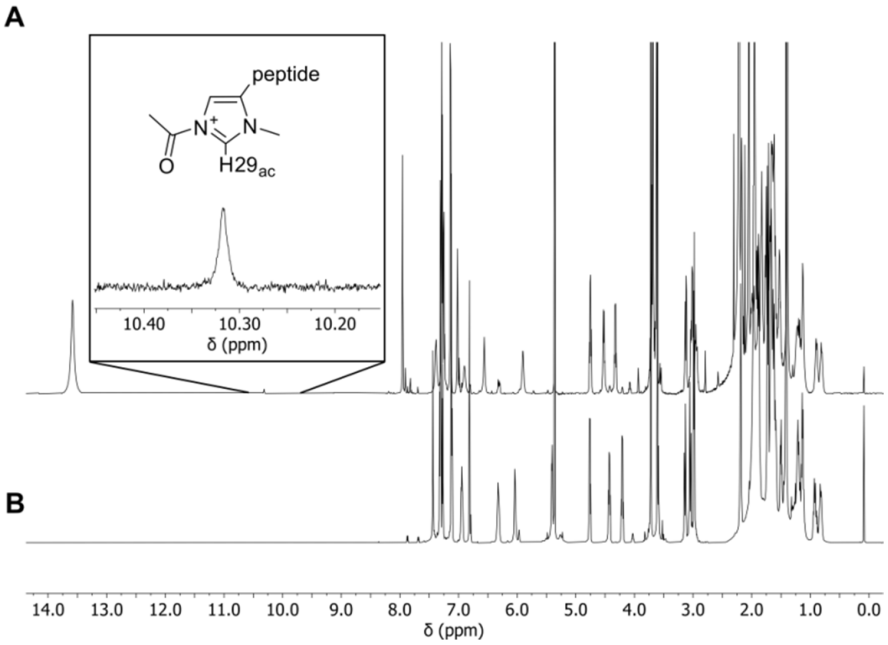

Figure 5. Full ^{1}H−NMR-spectra of tetrapeptide **1** without (**B**) and with (**A**) acetic anhydride **3** in DCM−d_2 at −20 °C (700 MHz ^{1}H frequency). Insert highlighting a new signal appearing after addition of acetic anhydride (ratio **3**:**1** = 7.11).

After having obtained the relevant ^{13}C chemical shift information, a ^{1}H-^{13}C-Heteronuclear Multiple Bond Correlation (HMBC) spectrum was recorded, which allows to link spin systems via the coupling between nuclei over more than one bond (Figure 6) [27] (Figures S9–S11).

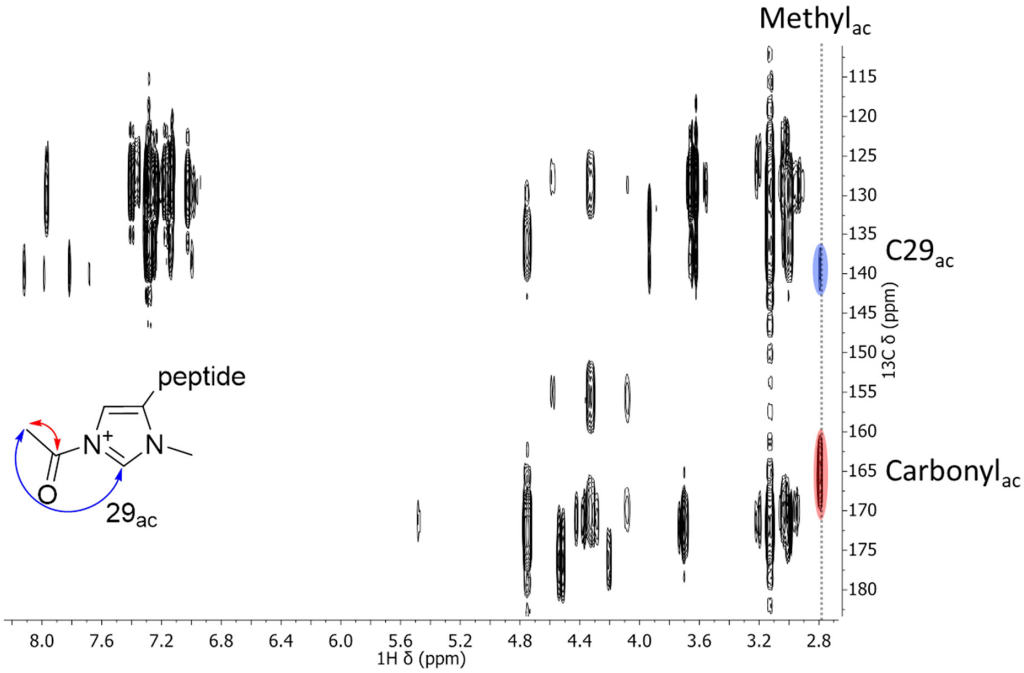

Figure 6. Excerpt of the ^{1}H−^{13}C-HMBC spectrum of tetrapeptide **1** and acetic anhydride **3** in DCM−d_2 at −20 °C (700 MHz ^{1}H frequency, 176 MHz ^{13}C frequency). Relevant signals are color coded and their correlations visualized. For the full spectrum see SI Figure S12.

A correlation of C29$_{ac}$ and a ^{1}H signal at 2.7 ppm is observed (blue). This ^{1}H signal is attributed to the methyl protons of the acetyl fragments considering its chemical shift, as

well as the other correlation the signal is showing (red). This other correlation with a ^{13}C resonating at 165 ppm is assigned to be one with the carbonyl carbon of the acetyl fragment. These observed correlations are indicative of a covalent bond between the acetyl fragment and the imidazolium ring and thus prove the existence and successful NMR-spectroscopic characterization of acetylated tetrapeptide **6**.

By addition of acetic anhydride **3**, the tetrapeptide/DCM-d_2 system re-equilibrates and the ^{1}H- as well as the ^{13}C-chemical shifts of the imidazole moiety change over time. As the system is observed while the reaction proceeds, the chemical shifts measured differ slightly between the HSQC and the HMBC.

For more evidence for the connectivity between the two fragments along with new insights into the dynamic process observed during the acylation of the tetrapeptide, selective ^{1}H Nuclear Overhauser Enhancement (NOE) spectra [28] were recorded (See supporting information Section S3.4 for experimental details). The resonances of H29, $H29_{ac}$, and $Methyl_{ac}$ were selectively irradiated and their correlations through NOE and chemical exchange are shown in Figure 7.

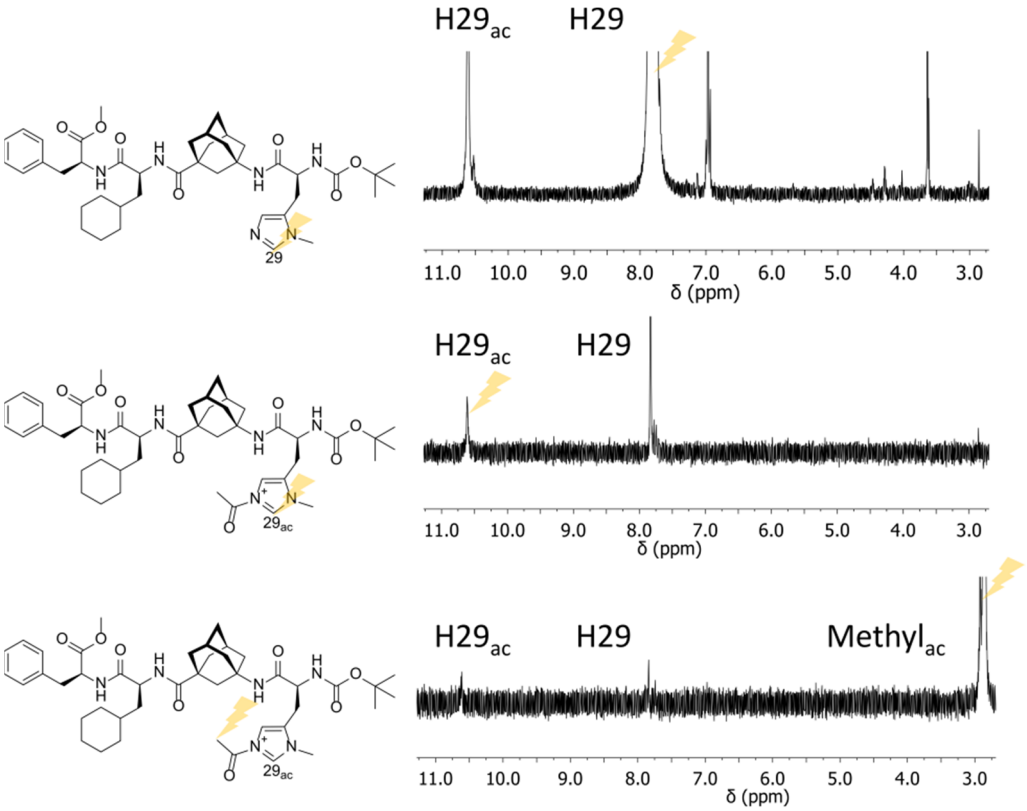

Figure 7. Selective $^{1}H-NOE$ spectra of tetrapeptide **1**, acetic anhydride **3** and acetylated tetrapeptide **6** in DCM$-d_2$ at -20 °C (700 MHz ^{1}H frequency).

Evidently, the imidazole proton H29 shows correlations with $H29_{ac}$ and $Methyl_{ac}$. The same interactions are found in the spectra of H29ac and $Methyl_{ac}$ (For spectra in toluene see supporting information Figures S13 and S14). Since the cross peaks bear the same phase as the diagonal peaks, this indicates that they are the result of exchange between the species. Depending on the correlation time of the compound, this conclusion can be misleading in the case of NOE spectra. It has been previously observed for the tetrapeptide that its correlation time is close to the one that leads to zero crossing of the NOE at 700 MHz [17]. For small molecules (in the case of exchange narrowing [29,30]) NOE (correlations through space) and chemical exchange (then termed EXchange SpectroscopY (EXSY) [31,32]) can be differentiated by their phase. The excited signals and the diagonal signals exhibit the opposite phase for NOE correlations while for chemical exchange they appear with the

same phase in the spectrum. For larger molecules (higher molecular weight and thus higher correlation time [33]) a zero crossing for the NOE occurs and in the slow motion limit [34,35] the signal phases in NOE experiments cannot discriminate between NOE and chemical exchange anymore. A remedy to this problem is provided by Rotating-Frame nuclear Overhauser Effect SpectroscopY (ROESY) spectra in which the cross relaxation does not change sign, due to its transversal nature such that spatial information and chemical exchange can be safely discriminated [36]. Efficient Adiabatic SYmmetrized Rotating-Frame nuclear Overhauser Effect SpectroscopY (EASY-ROESY) spectra were recorded for this reason [37]. The EASY-ROESY spectra confirm the exchange between the unacetylated and the acetylated terapeptide species (See supporting information Figure S15 for EASY-ROESY spectrum) and are thus evidence for tetrapeptide **1** being in equilibrium with the acetylated tetrapeptide **6** during the NMR experiment.

After detection of the different acylated tetrapeptides and verification of their structural connectivity, the next step is to actually follow the acetylation of the diol (Scheme 1). Thus, a solution of tetrapeptide **1** and acetic anhydride **3** in DCM-d_2 was prepared. The high solubility of **1** in DCM-d_2, combined with the fact that the acetylated tetrapeptide investigated here, shows the most intense signal of the acylated tetrapeptides, allows the study of its reaction with *R*,*R*-*trans*-cyclohexane-1,2-diol (*R*,*R*)**-2** using NMR-spectroscopy. A time series of 1D-^{1}H-spectra was recorded as a pseudo 2D-spectrum directly after adding (*R*,*R*)**-2** to a solution of **1** and **3**. Signals of the *R*,*R*-*trans*-cyclohexane-1,2-diol (*R*,*R*)**-2** (grey) vanish, while the signals of the acetylated diol **12** (green, blue and red) build up (Figure 8 (left)), resulting in the reaction profile shown in Figure 8 (right) (See supporting information Table S1 for sample composition). The signal intensity of the acetylated tetrapeptide **6** was constant over the course of the reaction. This reaction profile can be fit using DynaFit [38]. The best correlation with a low root-mean-square deviation (RMSD) of 0.21 mmol/L is obtained for a first order process. This suggests a direct acetylation of (*R*,*R*)**-2** by the acetylated tetrapeptide **6** under the conditions chosen (pseudo first order since acetic anhydride **3** is in large excess as ratio **3**:**1** = 12.20 and ratio (*R*,*R*)**-2**:**1** = 1.20) (See supporting information Figure S16 for first order fit and Figures S17 and S18 for zeroth- and second order fits for comparison).

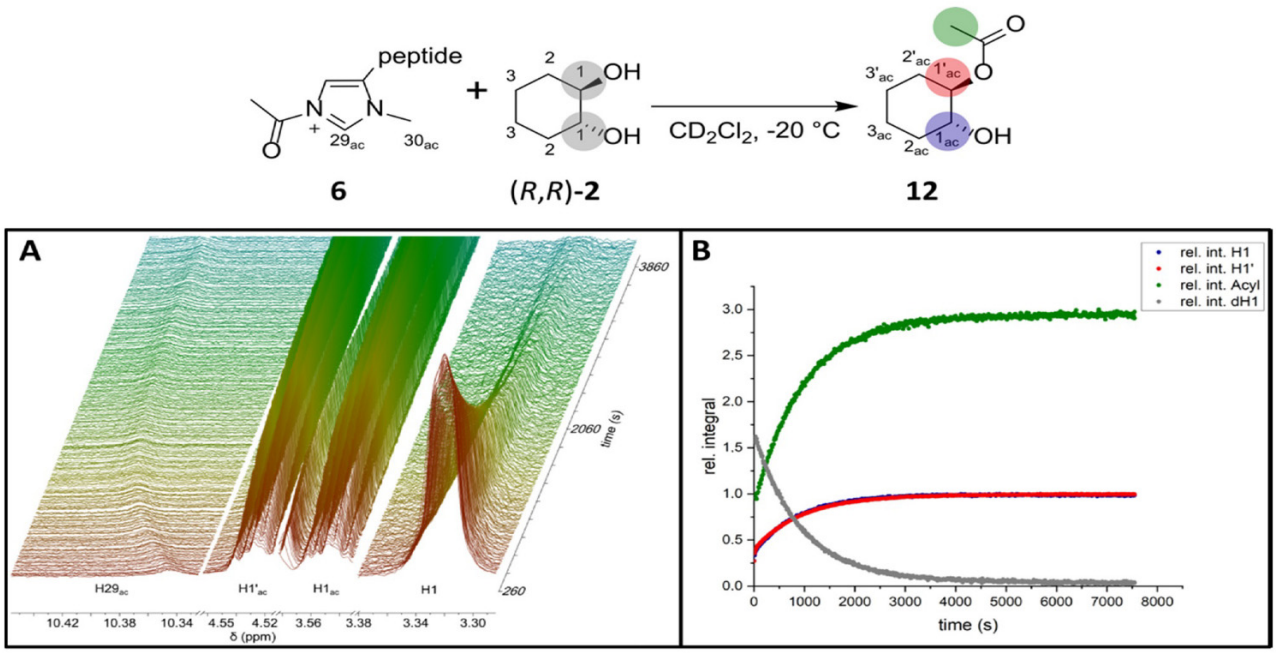

Figure 8. Stacked ^{1}H−spectra excerpts (700 MHz ^{1}H frequency) showing the course of the reaction for the selected signals $H29_{ac}$, $H1'_{ac}$, $H1_{ac}$ and H1 (**A**). Reaction profile of the acyl transfer from **6** onto **2** in DCM−d_2 at −20 °C (**B**).

3. Conclusions

We investigated the acyl-transfer by a highly selective tetrapeptide organocatalyst **1** onto *trans*-cyclohexane-diols. We employed different mass spectrometry techniques for the detection of acylated and unacylated species of tetrapeptide **1** alone and in complex with (acetylated) *trans*-cyclohexane-diols. The acylium ion of tetrapeptide **1** could be detected for all three anhydrides chosen. NMR spectroscopy was used to confirm the proposed acetylation site. The connectivity between the acyl fragment and peptide organocatalyst **1** could unambiguously be determined by HMBC. The acetylation takes place at the π-methylhistidine moiety as proposed previously. NMR was further used to monitor the reaction of the prepared catalyst. Under the conditions chosen (acetic anhydride **3** in excess) the signal of the acylium ion **6** could be observed throughout the reaction and its intensity remained constant. The detection of tetrapeptide **6** and the reaction product complexes is an important step towards the understanding of the highly enantioselective reaction of this organocatalyst.

Supplementary Materials: The following supporting information can be downloaded at: https://www.mdpi.com/article/10.3390/molecules27196351/s1. Figure S1: Positive ion mode (ESI+) spectrum of tetrapeptide 1 sprayed from DCM. Sample composition (Table S1). CID ESI-MS spectra of the acylated tetrapeptides (Figure S2; Figure S3) as well as a HCD spectrum of the reaction product complex of tetrapeptide **1**, acetic anhydride **3** and (*S*,*S*)**-2** (Figure S4). CID ESI-MS spectrum of tetrapeptide **1**+acetate (Figure S5). ^{1}H-NMR spectra of the acylated tetrapeptides (Figure S6; Figure S7). Full ^{1}H-^{13}C-HSQC- and ^{1}H-^{13}C-HMBC-spectra of the acetylated tetrapeptide (Figure S8; Figure S9), as well as selective 1D-^{1}H-NOE-spectra (Figure S10; Figure S11; Figure S12; Figure S13; Figure S14) and the full ^{1}H-^{1}H-EASY-ROESY spectrum (Figure S15). Fits of the reaction profile using zeroth, first and second order kinetics (Figure S17; Figure S16; Figure S18). Ref [11,17,22,26–28,36–42] are cited in the Supplementary Materials.

Author Contributions: M.B. Conceptualization: Lead; Data acquisition (NMR): Lead; Data acquisition (MS): Supporting; Data curation: Lead; Formal analysis: Lead; Data interpretation: Lead; Validation; Visualization; Original draft preparation; Review & Editing: Lead; T.H. Data acquisition (MS): Lead; Data interpretation: Supporting C.M.T. Project administration: Lead; Conceptualization: Lead; Data interpretation: Supporting; Review & Editing: Supporting; Funding acquisition. All authors have read and agreed to the published version of the manuscript.

Funding: This research was funded by the Deutsche Forschungsgesellschaft (DFG), grant number TH1115/12-1 and the Hans Messer Foundation.

Data Availability Statement: The data presented in this study are available on request from the authors.

Acknowledgments: C.M.T thanks the Deutsche Forschungsgesellschaft (DFG) for funding (TH1115/12-1). M.B. acknowledges funding by the Hans Messer Foundation and T.H. was supported by the Kooperative Promotionsplattform, financed by the Hessian Ministry of Higher Education, Research, and the Arts (HMWK). We thank Peter R. Schreiner and Raffael C. Wende (Justus Liebig University of Giessen) for providing the tetrapeptide.

Conflicts of Interest: The authors declare no conflict of interest.

Sample Availability: As all compounds—apart from the starting materials—are transient species only the starting materials can be provided upon request.

References

1. Yauk, Y.-K.; Souleyre, E.J.F.; Matich, A.J.; Chen, X.; Wang, M.Y.; Plunkett, B.; Dare, A.P.; Espley, R.V.; Tomes, S.; Chagné, D.; et al. Alcohol acyl transferase 1 links two distinct volatile pathways that produce esters and phenylpropenes in apple fruit. *Plant J.* **2017**, *91*, 292–305. [CrossRef] [PubMed]
2. Nachmansohn, D.; Machado, A.L. The formation of acetylcholine. A new enzyme: "Choline acetylase". *J. Neurophysiol.* **1943**, *6*, 397–403. [CrossRef]
3. Metrano, A.J.; Chinn, A.J.; Shugrue, C.R.; Stone, E.A.; Kim, B.; Miller, S.J. Asymmetric Catalysis Mediated by Synthetic Peptides, Version 2.0: Expansion of Scope and Mechanisms. *Chem. Rev.* **2020**, *120*, 11479–11615. [CrossRef]

4. Lewandowski, B.; Wennemers, H. Asymmetric catalysis with short-chain peptides. *Curr. Opin. Chem. Biol.* **2014**, *22*, 40–46. [CrossRef] [PubMed]
5. Wennemers, H. Asymmetric catalysis with peptides. *Chem. Comm.* **2011**, *47*, 12036–12041. [CrossRef]
6. Miller, S.J.; Copeland, G.T.; Papaioannou, N.; Horstmann, T.E.; Ruel, E.M. Kinetic Resolution of Alcohols Catalyzed by Tripeptides Containing the N-Alkylimidazole Substructure. *J. Am. Chem. Soc.* **1998**, *120*, 1629–1630. [CrossRef]
7. Jarvo, E.R.; Copeland, G.T.; Papaioannou, N.; Bonitatebus, P.J.; Miller, S.J. A Biomimetic Approach to Asymmetric Acyl Transfer Catalysis. *J. Am. Chem. Soc.* **1999**, *121*, 11638–11643. [CrossRef]
8. Jarvo, E.R.; Miller, S.J. Amino acids and peptides as asymmetric organocatalysts. *Tetrahedron* **2002**, *58*, 2481–2495. [CrossRef]
9. Copeland, G.T.; Miller, S.J. Selection of Enantioselective Acyl Transfer Catalysts from a Pooled Peptide Library through a Fluorescence-Based Activity Assay: An Approach to Kinetic Resolution of Secondary Alcohols of Broad Structural Scope. *J. Am. Chem. Soc.* **2001**, *123*, 6496–6502. [CrossRef]
10. Davie, E.A.C.; Mennen, S.M.; Xu, Y.; Miller, S.J. Asymmetric Catalysis Mediated by Synthetic Peptides. *Chem. Rev.* **2007**, *107*, 5759–5812. [CrossRef]
11. Müller, C.E.; Wanka, L.; Jewell, K.; Schreiner, P.R. Enantioselective Kinetic Resolution of trans-Cycloalkane-1,2-diols. *Angew. Chem. Int. Ed.* **2008**, *47*, 6180–6183. [CrossRef] [PubMed]
12. Müller, C.E.; Zell, D.; Hrdina, R.; Wende, R.C.; Wanka, L.; Schuler, S.M.M.; Schreiner, P.R. Lipophilic Oligopeptides for Chemo- and Enantioselective Acyl Transfer Reactions onto Alcohols. *J. Org. Chem.* **2013**, *78*, 8465–8484. [CrossRef] [PubMed]
13. Shinisha, C.; Sunoj, R.B. On the Origins of Kinetic Resolution of Cyclohexane-1, 2-diols through Stereoselective Acylation by Chiral Tetrapeptides. *Org. Lett.* **2009**, *11*, 3242–3245. [CrossRef] [PubMed]
14. Zhao, Y.; Truhlar, D.G. The M06 suite of density functionals for main group thermochemistry, thermochemical kinetics, noncovalent interactions, excited states, and transition elements: Two new functionals and systematic testing of four M06-class functionals and 12 other functionals. *Theor. Chem. Acc.* **2008**, *120*, 215–241. [CrossRef]
15. Wagner, J.P.; Schreiner, P.R. London Dispersion in Molecular Chemistry—Reconsidering Steric Effects. *Angew. Chem. Int. Ed.* **2015**, *54*, 12274–12296. [CrossRef]
16. Williamson, M.P. The Nuclear Overhauser Effect. In *Modern Magnetic Resonance*; Webb, G.A., Ed.; Springer: Dordrecht, The Netherlands, 2006; pp. 409–412.
17. Procházková, E.; Kolmer, A.; Ilgen, J.; Schwab, M.; Kaltschnee, L.; Fredersdorf, M.; Schmidts, V.; Wende, R.C.; Schreiner, P.R.; Thiele, C.M. Uncovering Key Structural Features of an Enantioselective Peptide-Catalyzed Acylation Utilizing Advanced NMR Techniques. *Angew. Chem. Int. Ed.* **2016**, *55*, 15754–15759. [CrossRef]
18. Alachraf, M.W.; Wende, R.C.; Schuler, S.M.M.; Schreiner, P.R.; Schrader, W. Functionality, Effectiveness, and Mechanistic Evaluation of a Multicatalyst-Promoted Reaction Sequence by Electrospray Ionization Mass Spectrometry. *Chem. Eur. J.* **2015**, *21*, 16203–16208. [CrossRef]
19. Ganem, B.; Li, Y.T.; Henion, J.D. Detection of Noncovalent Receptor-Ligand Complexes by Mass Spectrometry. *J. Am. Chem. Soc.* **1991**, *113*, 6294–6296. [CrossRef]
20. Hofstadler, S.A.; Sannes-Lowery, K.A. Applications of ESI-MS in drug discovery: Interrogation of noncovalent complexes. *Nat. Rev. Drug Discov.* **2006**, *5*, 585–595. [CrossRef]
21. Gadagkar, S.R.; Call, G.B. Computational tools for fitting the Hill equation to dose–response curves. *J. Pharmacol. Toxicol. Methods* **2015**, *71*, 68–76. [CrossRef]
22. OriginLab Corporation. *OriginPro 9.8.0*; OriginLab: Northampton, MA, USA, 2021.
23. Wan, K.X.; Gross, M.L.; Shibue, T. Gas-Phase Stability of Double-Stranded Oligodeoxynucleotides and Their Noncovalent Complexes With DNA-Binding Drugs As Revealed by Collisional Activation in an Ion Trap. *J. Am. Soc. Mass Spectrom.* **2000**, *11*, 450–457. [CrossRef]
24. Daniel, J.M.; Friess, S.D.; Rajagopalan, S.; Wendt, S.; Zenobi, R. Quantitative determination of noncovalent binding interactions using soft ionization mass spectrometry. *Int. J. Mass Spectrom.* **2002**, *216*, 1–27. [CrossRef]
25. Hesse-Ertelt, S.; Heinze, T.; Kosan, B.; Schwikal, K.; Meister, F. Solvent Effects on the NMR Chemical Shifts of Imidazolium-Based Ionic Liquids and Cellulose Therein. *Macromol. Symp.* **2010**, *294*, 75–89. [CrossRef]
26. Bodenhausen, G.; Ruben, D.J. Natural Abundance Nitrogen-15 Nmr by Enhanced Heteronuclear Spectroscopy. *Chem. Phys. Lett.* **1980**, *69*, 185–189. [CrossRef]
27. Bax, A.; Summers, M.F. Proton and carbon-13 assignments from sensitivity-enhanced detection of heteronuclear multiple-bond connectivity by 2D multiple quantum NMR. *J. Am. Chem. Soc.* **1986**, *108*, 2093–2094. [CrossRef]
28. Kessler, H.; Oschkinat, H.; Griesinger, C.; Bermel, W. Transformation of Homonuclear Two-Dimensional NMR Techniques into One-Dimensional Techniques Using Gaussian Pulses. *J. Magn. Reson.* **1986**, *70*, 106–133. [CrossRef]
29. Anderson, P.W. A Mathematical Model for the Narrowing of Spectral Lines by Exchange or Motion. *J. Phys. Soc. Jpn.* **1954**, *9*, 316–339. [CrossRef]
30. Sack, R.A. A contribution to the theory of the exchange narrowing of spectral lines. *Mol. Phys.* **1958**, *1*, 163–167. [CrossRef]
31. Jeener, J.; Meier, B.H.; Bachmann, P.; Ernst, R.R. Investigation of exchange processes by two-dimensional NMR spectroscopy. *J. Chem. Phys.* **1979**, *71*, 4546–4553. [CrossRef]
32. Nikitin, K.; O'Gara, R. Mechanisms and Beyond: Elucidation of Fluxional Dynamics by Exchange NMR Spectroscopy. *Chem. Eur. J.* **2019**, *25*, 4551–4589. [CrossRef]

33. Maciejewski, M.W.; Liu, D.; Prasad, R.; Wilson, S.H.; Mullen, G.P. Backbone Dynamics and Refined Solution Structure of the N-terminal Domain of DNA Polymerase β. Correlation with DNA Binding and dRP Lyase Activity. *J. Mol. Biol.* **2000**, *296*, 229–253. [CrossRef] [PubMed]
34. Otter, A.; Kotovych, G. The solution conformation of the synthetic tubulin fragment Ac-tubulin-α(430–441)-amide based on two-dimensional ROESY experiments. *Can. J. Chem.* **1988**, *66*, 1814–1820. [CrossRef]
35. Mirau, P.A.; Bovey, F.A. Two-Dimensional NMR Studies of Molecular Weight and Concentration Effects on Polymer-Polymer Interactions. *Macromolecules* **1990**, *23*, 4548–4552. [CrossRef]
36. Bothner-By, A.A.; Stephens, R.L.; Lee, J.; Warren, C.D.; Jeanloz, R.W. Structure Determination of a Tetrasaccharide: Transient Nuclear Overhauser Effects in the Rotating Frame. *J. Am. Chem. Soc.* **1984**, *106*, 811–813. [CrossRef]
37. Thiele, C.M.; Petzold, K.; Schleucher, J. EASY ROESY: Reliable Cross-Peak Integration in Adiabatic Symmetrized ROESY. *Chem. Eur. J.* **2009**, *15*, 585–588. [CrossRef] [PubMed]
38. Kuzmič, P. Chapter 10—DynaFit—A Software Package for Enzymology. In *Methods in Enzymology*; Johnson, M.L., Brand, L., Eds.; Academic Press: Cambridge, MA, USA, 2009; Volume 467, pp. 247–280.
39. Nehls, T.; Heymann, T.; Meyners, C.; Hausch, F.; Lermyte, F. Fenton-Chemistry-Based Oxidative Modification of Proteins Reflects Their Conformation. *Int. J. Mol. Sci.* **2021**, *22*, 9927. [CrossRef] [PubMed]
40. Thrippleton, M.J.; Keeler, J. Elimination of Zero-Quantum Interference in Two-Dimensional NMR Spectra. Angew. *Chem. Int. Ed.* **2003**, *42*, 3938–3941. [CrossRef]
41. Kupce, E.; Boyd, J.; Campbell, I.D. Short Selective Pulses for Biochemical Applications. *J. Magn. Reson. Ser. B* **1995**, *106*, 300–303. [CrossRef]
42. Fredi, A.; Nolis, P.; Cobas, C.; Parella, T. Access to experimentally infeasible spectra by pure-shift NMR covariance. *J. Magn. Reson.* **2016**, *270*, 161–168. [CrossRef]